A Graphical Approach to Examining Classical Extremum Seeking Using Bifurcation Analysis

Duc H. Nguyen, Mark H. Lowenberg, and Simon A. Neild

***Abstract*—The majority of extremum seeking literature discusses rigorous stability analysis, thereby limiting its audience to mathematicians and control engineers with strong theoretical backgrounds. Here, we complement these studies by proposing the use of harmonically-forced bifurcation analysis to evaluate parameter choices in classical extremum seeking systems. This method generates a graphical map of limit cycle attractors and how they change with respect to a chosen parameter. Our approach retains the full properties of a harmonically-forced system, thereby avoiding the requirement to approximate the dynamics as equilibrium solutions as done in previous studies. Common elements of nonlinear dynamical systems, such as loss of local stability and coexistence of multiple solutions via fold bifurcations are observed. Bifurcation analysis therefore provides an intuitive tool for engineers and new adopters to gain further insights into classical extremum seeking systems. The link between extremum seeking control and dynamical system theory is also highlighted. We use an example of an auto-trim system in a nonlinear, longitudinal (fourth-order) flight dynamics model to demonstrate the method. The influence of the forcing frequency, modulation phase, and high-pass filter frequency on the stability and performance of the system is examined using both one- and two-parameter continuation.**

***Index terms*—adaptive control, bifurcation, frequency response, nonlinear systems, stability analysis**

I. Introduction

EXTREMUM seeking control is a form of model-free adaptive control that automatically seeks out the extremum point(s) (maxima or minima) of an objective function. This is done via a 'perturb and observe' scheme, which injects a sinusoidal perturbation to the control signal and observes the subsequent changes in the objective function. An online estimation of the objective function slope can then be inferred, which in turn drives the control input to the point at which the slope is zero (i.e., the extremum). As the whole process is done online and does not require any knowledge of the plant, extremum seeking control is especially useful in cases where the optimal set point is either not known or is highly sensitive to changes in parameters, as often seen in many real-world applications.

Extremum seeking control has attracted significant attention from researchers in recent years. Specifically, the number of publications on the topic between 2000 and 2009 alone exceeded those from the year 1960 to 2000 combined [1]. Part of the reason for this sudden surge in interest is due to a pivotal paper in 2000, which provided the first rigorous mathematical proof of stability in a general nonlinear extremum-seeking system [2]. Since then, various engineering and industrial applications of extremum seeking control have been explored, including maximising pressure rise in an aero-engine compressor [3], optimising power output of wind turbines [4], and minimising power demand during formation flight [5], to name a few. On the theoretical front, some notable works include automatic tuning of PID gains [6], limit cycle amplitude minimisation [7], convergence analysis [8], and optimising systems with only periodic solutions [9]. Another recent development is the addition of a built-in extremum-seeking controller block in the R2021a release of the Simulink Control Design toolbox in MATLAB [10]. This reflects the increasing popularity of the method and will further introduce extremum seeking control to many new users through a user-friendly environment. For a formal introduction to extremum seeking control and its applications, readers are referred to papers [1, 11] and textbooks [12, 13].

Despite these developments, the current procedures for analysing an extremum-seeking system remain mathematically challenging and involve a number of assumptions that may prove impractical in many engineering systems. This in large part is due to the presence of the harmonic perturbation, which results in periodic motions and poses a challenge to both analytical and numerical analyses. Regarding the analytical side, the method of averaging and the singular perturbation method are employed to approximate the system under investigation as an equilibrium map [2]. The assumptions involved in these approaches require that the frequencies of the three main elements (the perturbation signal, the filters in the extremum controller, and the plant's dynamics) are well separated [7] – usually by an order of magnitude each. Considering the example of a generic flight dynamics model, these requirements are already limiting since a simple longitudinal (4^{th}-order) aircraft model with actuator already spans three orders of magnitude on the frequency spectrum: 10^{-1}–10^{0} rad/s for the two rigid-body modes and 10^{1} rad/s for the actuator. The impact of higher-order harmonic terms is also neglected in these approximations, which may further invalidate the results in highly nonlinear applications. More

Manuscript received March 22, 2022

All authors are with the Department of Aerospace Engineering, University of Bristol, Bristol, BS8 1TR UK.

Duc H. Nguyen (corresponding author, email: duc.nguyen@bristol.ac.uk)

Mark H. Lowenberg (email: m.lowenberg@bristol.ac.uk)

Simon A. Neild (email: simon.neild@bristol.ac.uk)

recently, the Lie bracket averaging method [14-16] can retain the harmonic-forcing dynamics, but this approach remains mathematically rigorous. On the computational front, recent works have successfully employed numerical continuation using the AUTO-07P software to analyse extremum seeking controllers [17-20]. Various nonlinear phenomena have been characterised using this continuation-based scheme, including existence of multiple stable solutions, unstable solutions, and loss of stability. However, the underlying equations of motion in [17-20] are still equilibrium approximations of the full harmonically-forced systems, so the assumptions listed above still apply.

To bridge this gap, we propose the use of harmonically-forced numerical continuation and bifurcation analysis to create a graphical representation of the possible dynamic responses in a classical extremum seeking system. Continuation provides a means to trace out paths of steady state solutions of a smooth (differentiable) dynamical system as one or more system parameters vary. The method can also infer local stability and trace out new solution branches arising from points where stability changes (bifurcation points). Accordingly, continuation can inform its users of the following features in a single diagram:

- Steady-state oscillation amplitude and stability.
- Potential existence of multiple solutions.
- Local stability boundaries.

Compared to previous studies using continuation [17-20], our approach does not approximate the steady-state response as equivalent equilibrium solutions (static, non-oscillatory). Therefore, all characteristics of a harmonically-forced system are retained, enabling the forcing-specific terms like forcing frequency and modulation phase to be investigated in terms of their impact on stability. Popular numerical continuation packages such as AUTO-07P [21] and COCO [22] can run these analyses in order of seconds or minutes. As such, our study provides an intuitive method for examining numerical applications that incorporate extremum seeking. It is expected that continuation, in the form presented in this paper, could be applied to other extensions of classical extremum seeking, such as multivariable extremum seeking [23, 24], slope-seeking controllers [25], and extremum seeking with periodic outputs [9, 26].

Lastly, it is worth mentioning that there are more advanced types of extremum seeking that have been developed in recent years (extremum seeking with delays [27, 28], for PDEs [29, 30], for hybrid systems [31, 32], and fractional-order extremum seeking [33, 34], etc.). Although we only examine classical extremum seeking in this study, there are extensions of continuation that can accommodate the richer dynamics in these advanced extremum seeking systems.

II. Problem Description

In this paper, we consider a fourth-order longitudinal aircraft model coupled with a conventional manoeuvre-demand controller and an auto-trim system – the latter uses extremum seeking. Although both controllers provide stability and accomplish their objectives, they have been intentionally tuned to achieve poor performance. This provides the backdrop to demonstrate the capability of harmonically-forced bifurcation analysis in identifying the stability boundaries and revealing the wide variety of dynamics that can be encountered in a highly nonlinear plant.

A. Aircraft model and the manoeuvre-demand controller

Fig. 1a shows the NASA's Generic T-tail Transport (GTT) model – the aircraft used in this study. The model was constructed based on a series of wind tunnel and water tunnel tests by NASA and Boeing [35-37] and represents a generic mid-sized regional jet airliner. In this paper, we constrain the aircraft's dynamics to the longitudinal plane (no rolling, yawing, or sideslip motions). Pitch control (nose up or down motion) is achieved using either the elevator or the all-moving horizontal tailplane – shown in Fig. 1a and Fig. 2. In practice, only the elevator is used for transient manoeuvres. Once the desired attitude is achieved, the elevator is brought back down to zero, and the tailplane replaces the elevator to generate the same pitching moment that keeps the aircraft at its current trajectory (i.e., trimming the aircraft). This arrangement minimises drag generated by the control surfaces (trim drag), mainly due to the large size of the tailplane that requires it to deflect at a smaller angle than the elevator does.

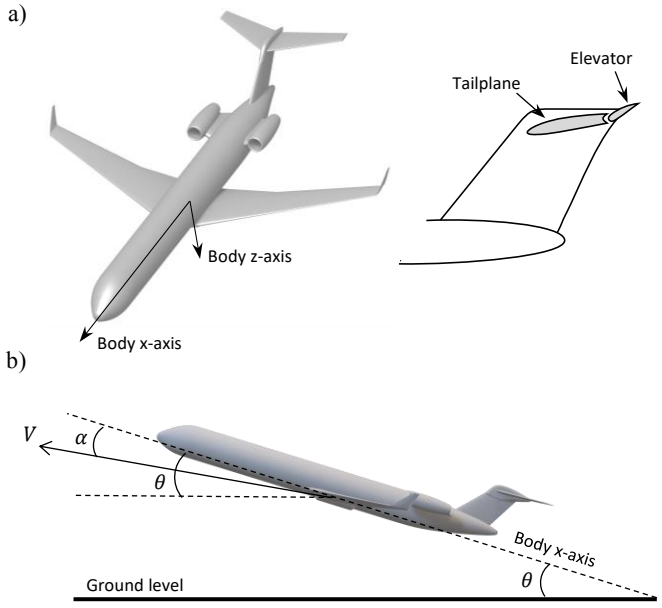

Fig. 1 The NASA Generic T-Tail Transport (GTT) and a side view of its tail assembly (a). Longitudinal flight dynamics notations (b).

Using the notation listed in Table I, the aircraft's dynamics in the vertical plane as shown in Fig. 1b can be described by the standard set of longitudinal equations of motion:

$$\dot{\alpha} = \frac{1}{mV}\left[\frac{1}{2}\rho V^2 S(C_z \cos\alpha - C_x \sin\alpha) - T\sin\alpha + mg\cos(\theta-\alpha)\right] + q \quad (1)$$

$$\dot{V} = \frac{1}{m}\left[\frac{1}{2}\rho V^2 S(C_z \sin\alpha + C_x \cos\alpha) + T\cos\alpha - mg\sin(\theta-\alpha)\right] \quad (2)$$

$$\dot{q} = \frac{1}{2}\rho V^2 Sc\frac{C_m}{I_y} - \frac{Th}{I_y} \quad (3)$$

$$\dot{\theta} = q \quad (4)$$

The coefficients of aerodynamic force along the body x and z axes C_x and C_z (forwards along the fuselage and downwards respectively) and the moment coefficient in pitch C_m are represented as follows:

$$C_i = C_{i_0}(\alpha) + C_{i_1}(\alpha, \delta_e, \delta_t) + C_{i_2}(\alpha)\frac{cq}{2V} \quad (5)$$

where $i = [x, z, m]$. The data for the terms in (5) are shown in Fig. 3, which use MATLAB's pchip and spline interpolation/extrapolation functions to make the model smooth for bifurcation analysis.

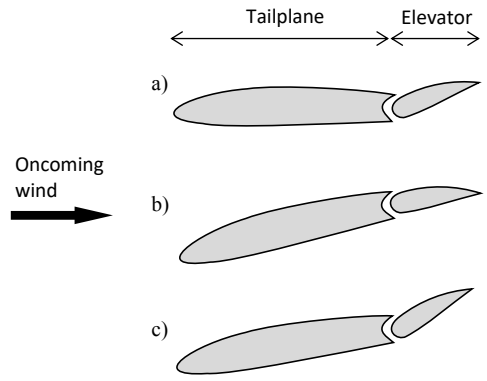

Fig. 2 Pitch control can be achieved my moving the elevator (a), the tailplane (b), or both (c). Figure shows negative tailplane and elevator deflections according to sign conventions, which generate a nose-up moment.

TABLE I. AIRCRAFT STATES AND PARAMETERS

α	angle of attack (rad)	STATES
V	velocity (m/s)	
q	pitch rate (rad/s)	
θ	pitch angle (rad)	
δ_e	elevator deflection (deg)	INPUTS
δ_t	tailplane deflection (deg)	
C_x	Body x-axis force coefficient	COEFFICIENTS
C_z	Body z-axis force coefficient	
C_m	pitching moment coefficient	
c	mean aerodynamic chord	3.37 m
g	gravitational acceleration	9.81 m/s^2
h	thrust line distance above CG	2.02 m
I_y	pitch moment of inertia	1,510,624 kg m^2
m	mass	25,332 kg
S	wing area	70.1 m^2
T	thrust	29,982 N
ρ	air density (at 10,000 ft)	0.905 kg/m^3

In this paper, the GTT is coupled to two separate controllers as shown in Fig. 4:

- The manoeuvre-demand controller calculates the elevator deflection δ_e so that the angle of attack α matches the reference signal α_d (demanded α). This is done by subtracting α from α_d in the outer loop, multiplying this signal by gain K_I, and then integrating it. In the inner loop, a proportional stability augmentation system is included using pitch rate q and pitch angle θ feedback, providing pitch damping and stiffness, respectively. The values of all three gains K_I, K_q, and K_θ are fixed.
- The extremum-seeking controller C_E (Fig. 4b) observes changes in δ_e and calculates the necessary tailplane deflection δ_t. This is used for the auto-trim function. The details of this scheme are presented in the next section.

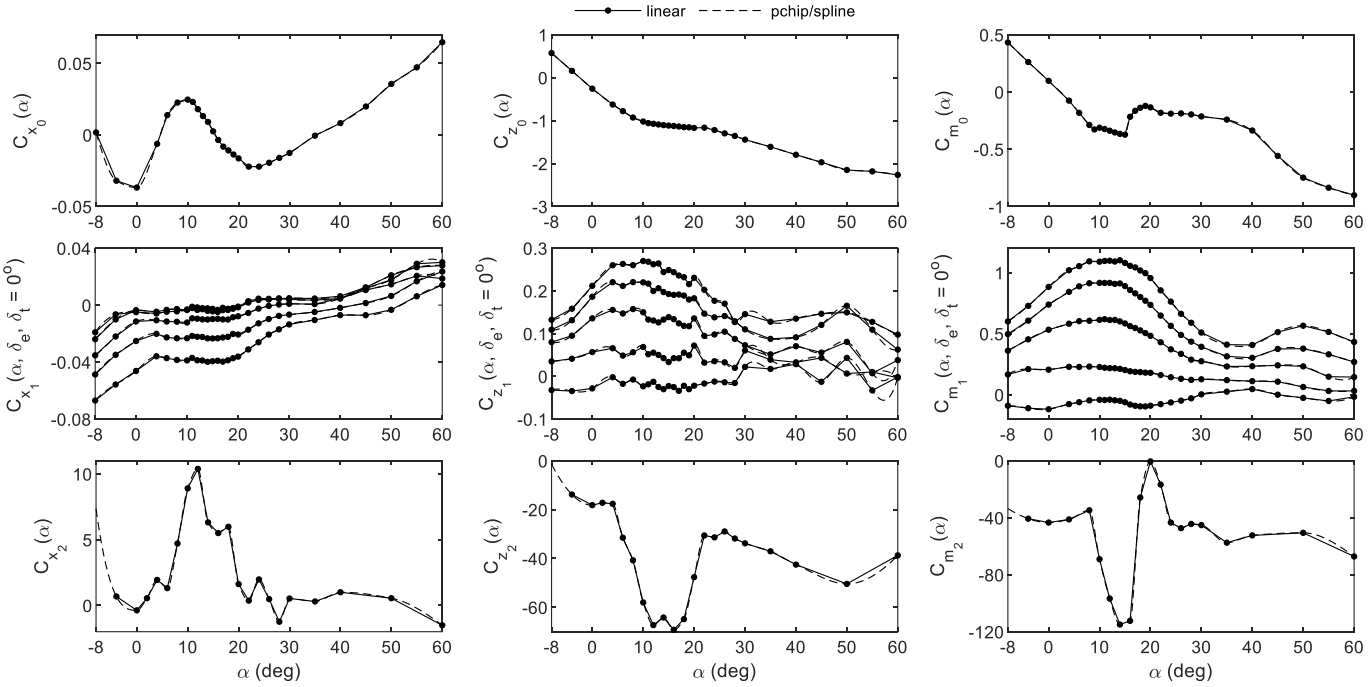

Fig. 3 Aerodynamic coefficients of the GTT.

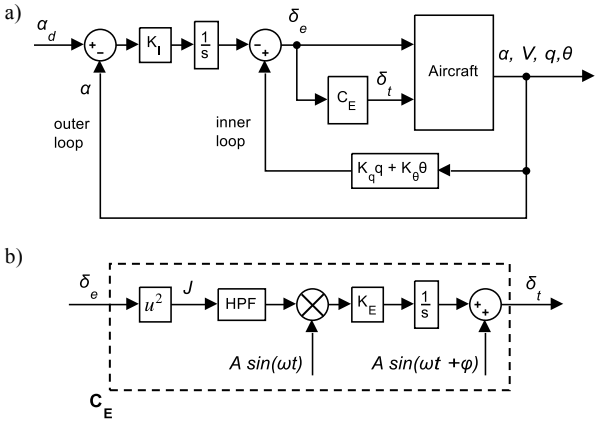

Fig. 4 Closed-loop block diagrams.

As mentioned, the closed-loop system is stable, although the gains have been selected to give poor performance.

B. The extremum-seeking auto-trim controller

An extremum-seeking controller will automatically seek out the maxima or minima of an objective function, which are the points with zero slopes. In this example, the objective function is defined as $J = \delta_e^2$. The idea is that the controller will adjust the tailplane deflection δ_t until δ_e^2 reaches its minimum at zero. When this condition is achieved, the aircraft will be flying at the commanded angle of attack using only tailplane for trim and may represent minimum trim drag.

Since pitch control can be achieved using either elevator or tailplane deflection, there are multiple combinations of these control inputs that can be used to keep the aircraft flying at a constant angle of attack. The static relationship between elevator and tailplane deflections that maintains flight at α = 2 deg is shown as the solid line in Fig. 5a, with the inset showing a magnified view. This value of α was chosen because it is indicative of trimmed horizontal flight in normal operation. The tailplane is physically limited to deflecting between –10 and +5 deg, so its aerodynamic data in only available within that range. However, the data can be spline-extrapolated as shown by the dashed lines. This artificially creates a peak and a trough with zero slopes that can potentially draw the auto-trim controller toward them instead of the desired δ_e^2 = 0 point. For our purpose, this artificial peak/trough pair is desirable as it allows us to demonstrate the full capability of continuation methods in identifying additional attractors that may be hard to detect. Therefore, spline extrapolation is used for the tailplane aerodynamic data. This results in the objective function $J = \delta_e^2$ as shown in Fig. 5b, with the three zero-slope points labelled A-C; point B is the desired target for the auto-trim controller.

A brief introduction to the principles of extremum seeking control is now presented, although readers are referred to sources such as [12, 13] for a more formal introduction. Figure Fig. 4b is the block diagram of the auto-trim controller. The input to the controller is elevator, which is automatically controlled by the α-demand system. $J = \delta_e^2$ is the objective function as defined, which passes through a high pass filter to remove the bias. This signal is multiplied by a sinusoidal perturbation of the form $A\sin(\omega t)$ and a proportional gain K_E and then integrated. Finally, another sinusoidal perturbation is added with a phase lag ϕ, giving us the tailplane deflection δ_t as the output. In this scheme, the controller will continuously perturb the tailplane at a frequency ω rad/s, thereby causing J to vary sinusoidally at the same frequency. The α-demand controller will adjust δ_e in response to changes in δ_t by following the static map in Fig. 5a to keep the angle of attack at 2 deg. The set point of δ_t is determined by the integral action, which continuously drives δ_t until the signal between K_E and the integrator oscillates symmetrically about zero. This only happens when J reaches one of the inflection points in Fig. 5b (so that the product of $J(\omega t)$ and A $\sin(\omega t)$ is symmetric about zero). The extremum seeking controller therefore has the capability to automatically seek out an inflection point in an objective function without any knowledge of the model – making it especially useful for plants that are sensitive to changes in system parameters. We acknowledge that a real-world auto-trim controller does not require extremum seeking [38-40], and the example provided here is only to demonstrate the capability of bifurcation and continuation methods in analysing an extremum-seeking system.

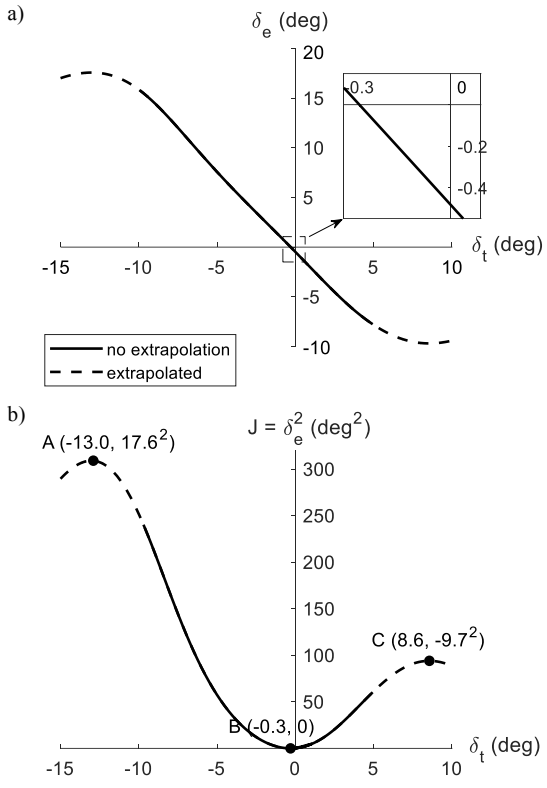

Fig. 5 Static map between elevator and tailplane for trimmed flight at α = 2° (a) and the objective function (b).

III. Overview of Bifurcation Methods and Numerical Continuation

Bifurcation and continuation methods are used to examine the dynamics of the closed-loop GTT mathematical model in this paper. A brief description of these methods is now presented. Consider a general autonomous dynamical system of the form:

$$\dot{\boldsymbol{x}} = f(\boldsymbol{x}, \boldsymbol{u}) \tag{6}$$

where f is a vector of n smooth (differentiable) functions, $\boldsymbol{x}$ is the state vector of dimension $(n \times 1)$ and $\boldsymbol{u}$ is the input vector. For the open-loop GTT aircraft, f contains the equations of motion (1-4), $\boldsymbol{x} = [\alpha, V, q, \theta]$, and $\boldsymbol{u} = [\delta_e, \delta_t]$. The system is in equilibrium when

$$\dot{\boldsymbol{x}} = \boldsymbol{0} \tag{7}$$

or is in a limit cycle of period T when

$$\boldsymbol{x}(t) = \boldsymbol{x}(t + T) \tag{8}$$

By solving equation (7) and/or equation (8), a map of steady state solutions (equilibrium or periodic) as functions of one of the control inputs in $\boldsymbol{u}$ can be generated. This map is referred to as a bifurcation diagram. The equations are solved numerically using a continuation method [41], which utilises a path-following algorithm to trace out a map of solutions as a parameter in $\boldsymbol{u}$ is varied. This varying parameter is referred to as the continuation parameter. Numerical continuation requires knowledge of at least one solution, which can be obtained by the user using time integration (simulating the system long enough so that the states converge to their final values, assuming the system is stable) or Newton's method. In many published works, the terms 'bifurcation analysis' and 'numerical continuation' are used interchangeably.

Local stability is determined by examining the eigenvalues or the Floquet multipliers for every steady state solution of the linearised system. A bifurcation arises when stability is lost, leading to nonlinear behaviour such as multiple solutions for the same input or hysteresis, depending on the type of bifurcation encountered. The mathematical definition of a bifurcation is:

- For equilibrium solutions: when at least one eigenvalue of the system's Jacobian matrix $J = df/dx|_{x_0}$ (evaluated at the equilibrium point x_0) crosses the imaginary axis.

- For periodic solutions: when a Floquet multiplier crosses the unit circle.

In this paper, time simulation is used to verify the local stability predictions. If the initial conditions of the simulation are not sufficiently close to the predicted stable solutions, there is a chance that the system would diverge to infinity or converge to an undetected branch, possibly an isolated attractor. Examining the global stability of extremum seeking systems is a separate topic for further studies

Fig. 6 shows an example bifurcation diagram of the open-loop GTT. This is essentially a map of all trim points at different elevator positions. It can be seen that for δ_e between –6.6 and –4.9 deg, there are three equilibrium solutions (two stable and one unstable) due to a pair of fold bifurcations. Furthermore, the insets highlight two small regions of limit cycles (self-oscillation). The Hopf bifurcations bounding the limit cycle regions are also shown. Note that for the family of unstable limit cycles near α = 17 deg, only one Hopf bifurcation was discovered. This branch of unstable periodic solutions terminates by colliding with the equilibrium branch via a global (homoclinic) bifurcation. Note that it is also possible to produce so-called two-parameter bifurcation diagrams, which follow the loci of bifurcation points as two parameters vary; these indicate regions in parameter space with varying number of possible solutions.

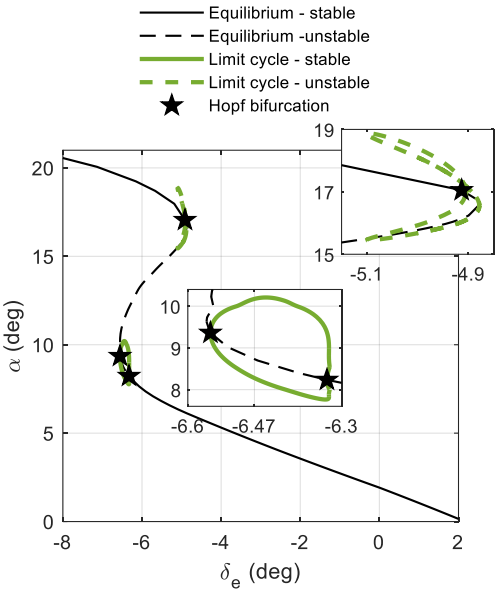

Fig. 6 Bifurcation diagram of the open-loop GTT at δ_t = 0°. Insets show magnified views near the Hopf bifurcations.

Numerical continuation requires that the state equations are written in autonomous form (no t on the right-hand side of (6)). To use continuation in a harmonically-forced system, the term $\sin \omega t$ is replaced by x_1, defined as

$$\dot{x}_1 = \quad x_1 + \omega x_2 - x_1(x_1^2 + x_2^2) \tag{9}$$

$$\dot{x}_2 = -\omega x_1 + x_2 - x_2(x_1^2 + x_2^2) \tag{10}$$

It can be shown that $x_1 = \sin \omega t$ and $x_2 = \cos \omega t$ are asymptotically stable solutions of (9-10) (see the appendix of [42]). Mathematically speaking, this transformation has effectively converted a harmonically-forced system into a self-oscillating plant by adding two 'dummy states' (9-10), thereby satisfying the requirement of (6) being in autonomous form. As long as the initial conditions of x_1 and x_2 are 0 and 1, the time-integrated responses using (9-10) should be identical to using $\sin \omega t$ for the forcing term.

The modulation and demodulation signals in a classical extremum seeking system can have a phase lag ϕ. To reflect the contribution of ϕ (in rad) in the harmonic forcing term, we combine x_1 and x_2 to generate the modulation/demodulation signal using (11)

$$\sin(\omega t + \phi) \equiv \quad x_1 \cos\phi + x_2 \sin\phi \tag{11}$$

For demonstration, the open-loop frequency response of the GTT at α = 2° can be obtained by setting δ_t = 0, $\delta_e = -0.48 + 0.2x_1$, and choosing ω as the continuation parameter (noting that –0.48 deg is the elevator deflection required for trim at 2° angle of attack, and 0.2 ° is an arbitrarily-chosen small forcing

amplitude). After some further post-processing of the periodic solutions using the approach outlined in [43], the nonlinear frequency response can be generated as shown in Fig. 7. A conventional 4th-order aircraft like the GTT has two natural dynamic modes known as short-period and phugoid. They are visible as two distinct peaks that are usually separated by an order of magnitude. These two modes will be referred to in later discussions.

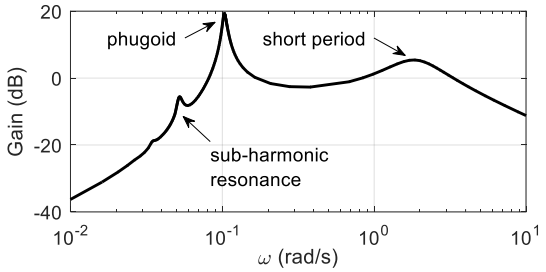

Fig. 7 Open-loop nonlinear δ_e-to-α frequency response at 0.2 deg elevator forcing amplitude obtained using continuation. Sub-harmonic resonance is caused by nonlinearities in the system and is therefore not observable in a conventional Bode plot.

All bifurcation diagrams in this paper were numerically generated in the MATLAB/Simulink environment using the Dynamical Systems Toolbox [44], which is the MATLAB implementation of the continuation software AUTO-07P [21]. Details of the numerical algorithm in AUTO can be found in [45, 46].

IV. Results and Discussions

A. Stability analysis and frequency dependency

For initial analysis, the values listed in Table II are used in the extremum seeking auto-trim controller.

TABLE II. Extremum Seeking Controller Parameters

A	forcing amplitude	0.2 deg
K_E	learning rate	5
ϕ	demodulation phase	90 deg
ω_F	high-pass filter cutoff frequency	6 rad/s

Consider the trimmed aircraft at α = 1 deg, which requires $[\delta_e, \delta_t] = [0, 0.4]$ deg. Then, apply a 1 deg step input in the demanded angle of attack to raise α to 2 deg. The resulting responses under two different forcing frequencies are shown in Fig. 8. In the 5.0 rad/s case, after the initial transient dynamics dominated by the α-demand controller (roughly the first 100s), the auto-trim system gradually exchanges elevator for tailplane, eventually bringing elevator down to zero as desired. At this point, the aircraft maintains its 2-degree angle of attack trajectory using only the tailplane. If the forcing frequency is reduced to 2.3 rad/s, the auto-trim controller is unable to bring the elevator down to zero, and the tailplane and elevator converge to a different combination that still keeps the aircraft flying at 2 deg angle of attack (but in a higher drag condition).

These two different responses suggest that there are at least two stable attractors. Bifurcation analysis is now used to trace out families of these solutions as the forcing frequency ω varies. The resulting bifurcation diagrams of the elevator and stabilator deflections are shown in Fig. 9, in which panel a is the overall view and panels b and c are the magnified views. By setting the forcing frequency ω on the x-axis, we can examine how the choice of ω affects the oscillation amplitude and stability. All solutions in Fig. 9 are limit cycles, and both the maxima and the minima of the oscillation are shown (although the amplitudes are small, so the maxima and minima are almost indistinguishable, apart from those in panel b). Since the oscillation amplitudes can be identified on the diagram, bifurcation methods provide a major advantage over existing methods that approximate the responses as equilibrium maps. The colours indicate whether the solutions belong to the same family and can therefore be detected in one continuation run. In this instance, two separate branches are detected, which are henceforth referred to as the red and blue branches.

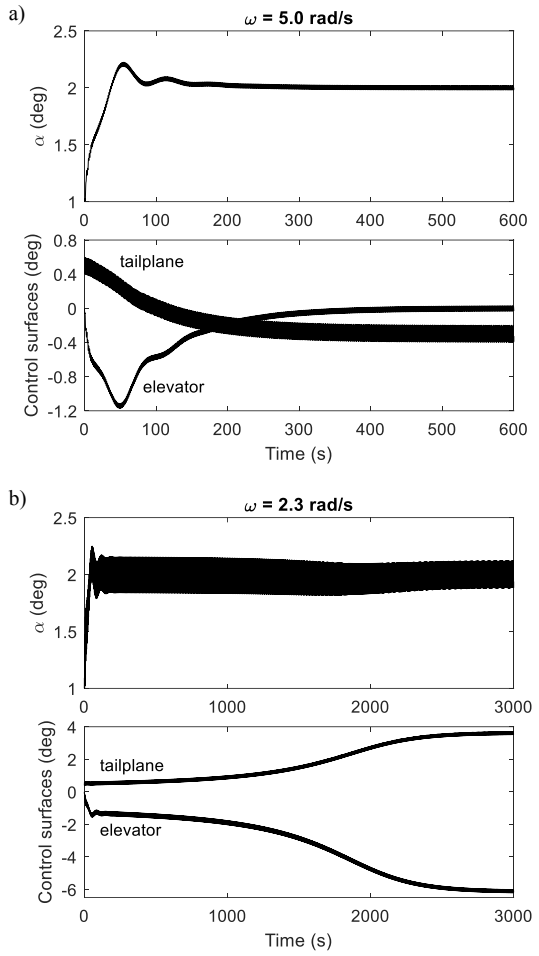

Fig. 8 Responses to step change in α_d using two different forcing frequencies.

Panels c indicate that when ω is between 1.8 and 2.34 rad/s (noting that 2.34 rad/s is the x-coordinate of point F), there are stable solutions from both the red and blue branch. At frequencies where both the red and blue stable solutions coexist, the initial conditions will determine which solution the aircraft converges to. Beyond 2.34 rad/s, there is only one stable solution from the blue branch that corresponds to peak B in Fig. 5b – the desirable one, whereas the solutions on the red branch

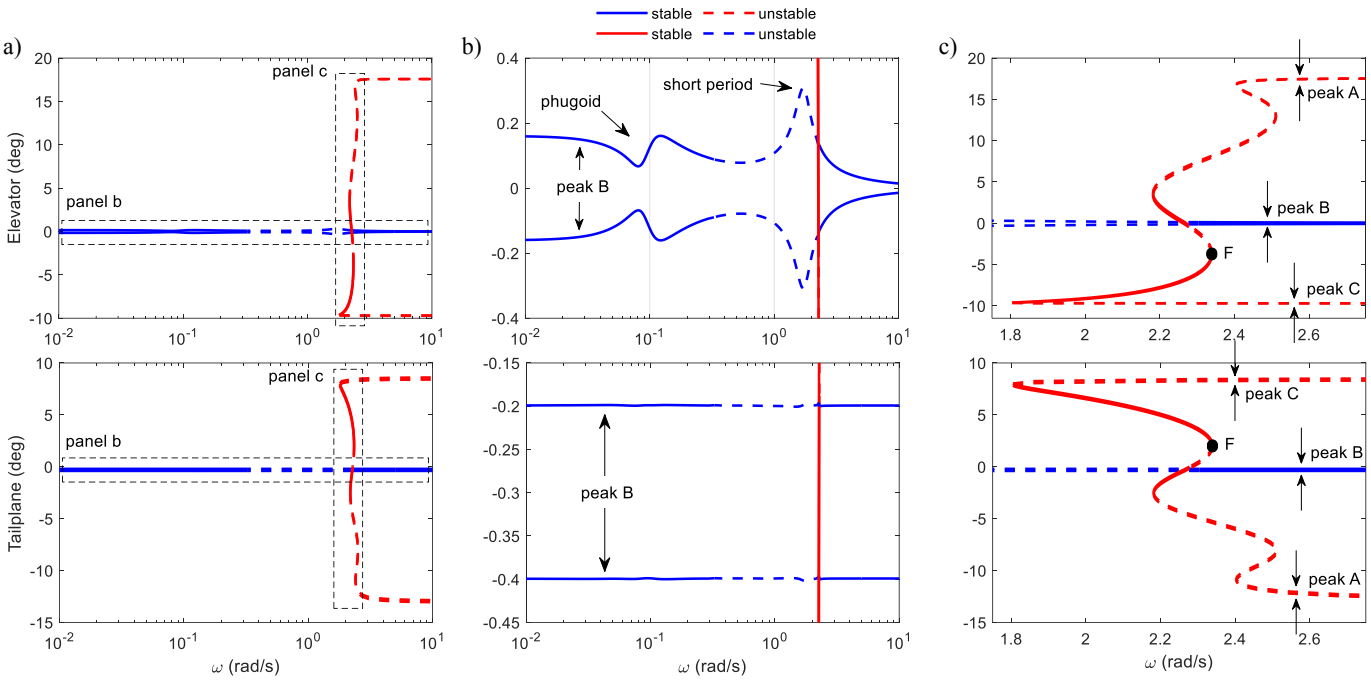

Fig. 9 Bifurcation diagrams – ω continuation. Panels b and c are the magnified views of panel a.

for peak A and C at these frequencies are unstable. It will be shown later that without the high-pass filter (the HPF block Fig. 4b), these solutions can be stable and result in a controller that is far more susceptible to converging to peaks A or C. It is also noted that the red and blue branches cross each other at a point that resembles a transcritical bifurcation, although the crossing point is not detected by the continuation solver.

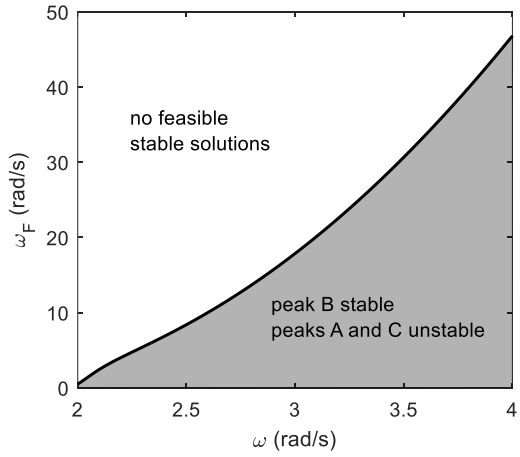

Fig. 10 Two-parameter continuation of point F.

Point F in panel c is the boundary of ω that ensures the blue branch is the only stable solution, which is desirable during operation (unless ω is reduced to below 0.33 rad/s, at which point the blue branch becomes stable again but results in responses that are too slow to be viable). The location of point F is sensitive to the filter cutoff frequency ω_F. To investigate this, we trace out the locus of point F on the ω-ω_F plane using two-parameter continuation as shown in Fig. 10. This diagram helps us determine the minimum safe operating frequency. By staying to the right side of this boundary, it is likely that the stable solutions of the blue branch are the only stable attractor present, and this helps us determine the safe operating region for the auto-trim controller. To further ensure stability, it is good practice to extend the continuation parameter range in Fig. 9 beyond the expected values where the system operates. This is because in some instances, the solutions may reverse direction via a fold bifurcation and re-enter the reasonable parameter space (see Fig. 3a in [47] for an example). Two-parameter continuation can then be used to follow this new fold bifurcation.

The nature of the instabilities in the blue branch is now examined. In the elevator response in Fig. 9b, two resonance frequencies are observed that match the short-period and phugoid frequencies in the open-loop frequency response (Fig. 7). Therefore, it can be said that these instabilities are caused by the extremum seeking controller forcing the system at the short-period frequency. It is known that the forcing frequency should be well-separated from the natural frequencies. However, continuation can determine the exact forcing frequencies at which instabilities can occur. We can also see here that it is safe to operate around the phugoid frequency because no instability is detected. To sum up, continuation provides a powerful capability for extremum seeking controller design and parameter tuning, especially in highly nonlinear systems that may not provide sufficient frequency separations.

B. Continuation in ϕ

We will now further illustrate how parameter choices can affect stability. As a demonstration, the demodulation phase ϕ is chosen as the continuation parameter. The effects of ϕ on stability and performance have not been thoroughly examined in the literature, so this provides the backdrop to demonstrate the capabilities of continuation.

In section IV-A where ϕ = 90 deg, it has been shown that the only stable attractor at ω = 5 rad/s comes from the blue branch that corresponds to peak B. We now fix ω at 5 rad/s and select

ϕ as the continuation parameter. The resulting bifurcation diagram is shown in Fig. 11, which has the following notable features:

- The blue branch is stable in the region $-55^o < \phi < 125^o$. Generally speaking, there is a 180^o window for ϕ that keeps the system stable.

- Beyond this region, the blue branch becomes unstable, and a new branch coloured grey is detected. In this branch, the solutions linked to peaks A and C are stable.

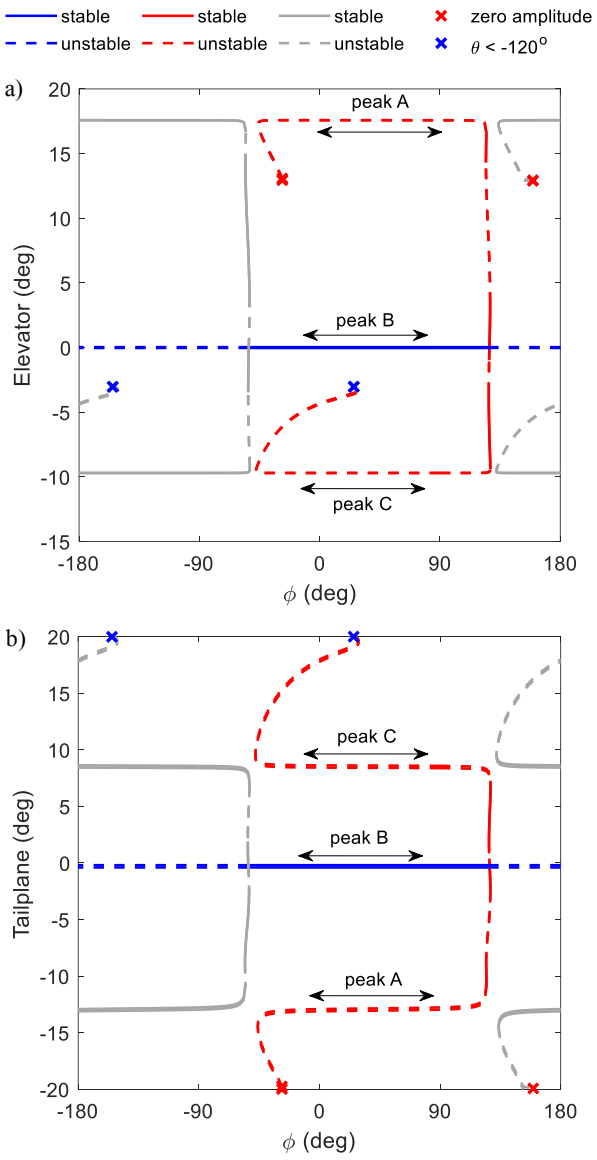

Fig. 11 Bifurcation diagram – ϕ continuation. ω is fixed at 5 rad/s. Note that all solutions are repeated for every 360 deg interval.

The continuation algorithm encounters numerical issues when solutions beyond the red and blue crosses are calculated. In the case of the former, the oscillation amplitude goes to zero, suggesting that the branch is crossing a family of equilibrium solutions at which the extremum controller is not active. With the latter (blue cross), it was found that these unstable solutions have the pitch angle θ below –120 deg, which is highly unrealistic. These results are not deemed of importance, and we therefore do not pursue solutions beyond these two crosses.

To determine the value for ϕ within the blue region that gives the most stable response, we examine the movement of the Floquet multiplier closest to the unit circle as ϕ varies (noting that the system becomes unstable when a Floquet multiplier crosses the unit circle). This is shown in Fig. 12 as the 5.0 rad/s line, indicating that ϕ = 37 deg is the most stable. We verify this by comparing the ϕ = 37 deg and 90 deg responses in time simulations as shown in Fig. 13a. It can be seen that ϕ = 37 deg gives a more stable and faster convergence as predicted, making it the most optimal demodulation phase at 5 rad/s forcing.

The Floquet multiplier movement at a lower forcing frequency of 2.1 rad/s is also shown in Fig. 12. It can be seen that the most stable point has shifted slightly to ϕ = 31 deg. Furthermore, the shape of the Floquet movement has changed significantly near the most stable point, indicating that a different Floquet multiplier is approaching the unit circle. Another notable feature here is that by reducing the forcing frequency, the system is actually more stable and converges faster, as long as the demodulation frequency is adjusted accordingly. This is verified in Fig. 13b, which shows the extremum seeking controller converging to its final value at a much earlier point than the ω = 5.0 rad/s case. It is also worth noting that stability is now achieved at 2.1 rad/s forcing. This is lower than the 2.3 rad/s case presented previously (Fig. 8), in which the system failed to converge to the desirable solution due to the non-optimised value of ϕ.

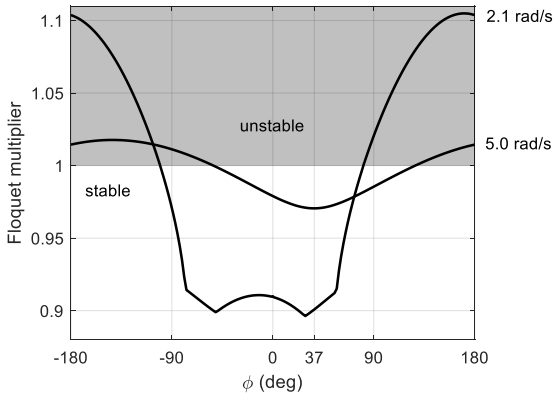

Fig. 12 Variation of the Floquet multiplier closest to the unit circle at two different forcing frequencies. Responses with Floquent multiplier above 1 are unstable.

By repeating the calculations in Fig. 11 and Fig. 12 at different forcing frequencies, we can track the movement of the blue branch's stability boundary as well as the point with the lowest Floquet multiplier. The result is shown in Fig. 14, which indicates that in general, the most stable point is right in the middle of the stability boundary, although this is no longer true for lower forcing frequencies when another Floquet multiplier approaches the unit circle at a faster rate, leading to the off-centred location of the most stable point.

The results so far seem to suggest that a lower forcing frequency is better due to the faster response and higher degree of stability. However, this comes with a trade-off. Fig. 15 shows that although the Floquet multiplier reduces with ω, the oscillation amplitude is actually increasing exponentially. The

larger oscillation due to lower forcing frequency can be clearly seen in Fig. 13, and this provides another indication of the upcoming instability as the forcing frequency approaches the short-period frequency.

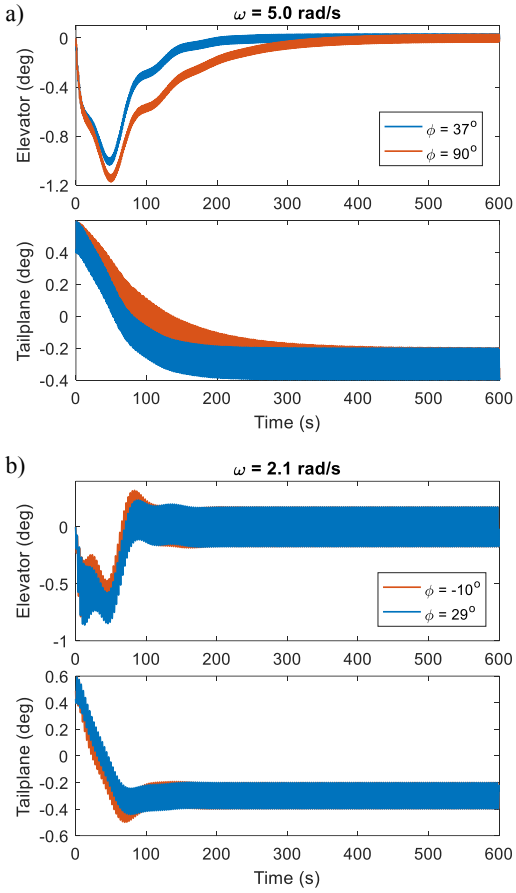

Fig. 13 Time simulations at 5.0 rad/s forcing (a) and 2.1 rad/s (b). In (b), ϕ = –10° lies halfway between the stability boundaries but ϕ = 29° the fastest-converging solution – as correctly predicted in Fig. 12.

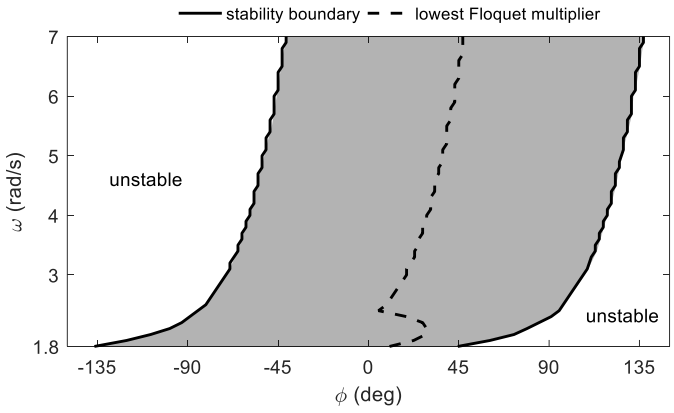

Fig. 14 Movement of the blue branch's stability boundary region and the most stable point.

Lastly, we examine the dynamics at an even lower forcing frequency. Fig. 16 is the magnified bifurcation diagram at ω = 1.7 rad/s. In this instance, the red and blue branches merge with each other in what looks like an imperfect transcritical bifurcation (hence the change of colour to black, as the red/blue distinction is no longer applicable). This marks a notable qualitative change in the system dynamics and suggests that the forcing frequency is getting too close to the short-period frequency. To maintain both stability and performance, the controller therefore should not operate below 1.8 rad/s forcing, which is the lowest value for ω before the imperfect transcritical bifurcation occur.

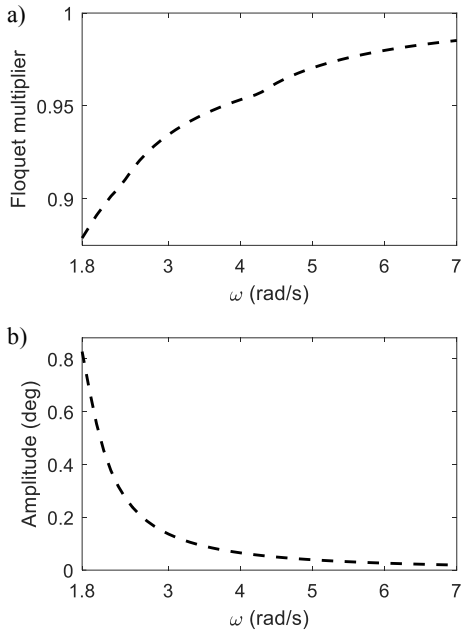

Fig. 15 Variation in the Floquet multiplier and α oscillation amplitude of the dashed line in Fig. 14.

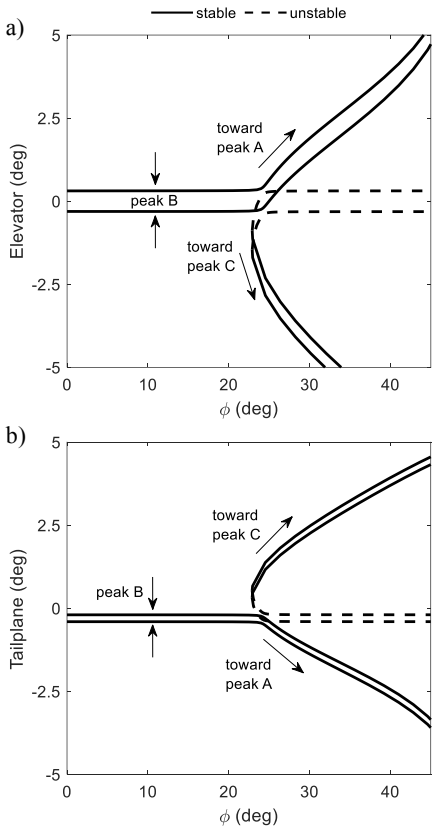

Fig. 16 ϕ continuation at ω = 1.7 rad/s.

This article has been accepted for publication in IEEE Transactions on Control Systems Technology. This is the author's version which has not been fully edited and content may change prior to final publication. Citation information: DOI 10.1109/TCST.2023.3242199

C. Dynamics without the high-pass filter

For the final analyses, the high-pass filter is removed whilst the remaining parameters are kept at their original values shown in Table II. We also modify the objective function slightly to $J = |\delta_e|$ as shown in Fig. 17. This was found to extend the stable regions of all three peaks compared to using the previous objective function $J = \delta_e^2$, which makes it easier to present the results without loss of generality. With this new J, peak B* is the desirable operating point. Although the transition between left- and right-side of B* is no longer smooth due to the absolute value function, continuation can still generate the full bifurcation diagram, illustrating that the method is still applicable in some instances with non-smooth objective functions.

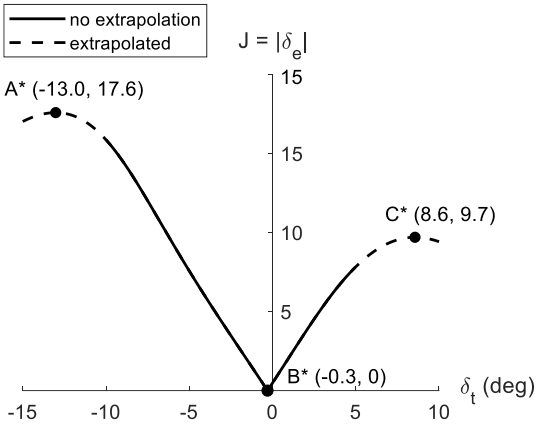

Fig. 17 Modified objective function.

Setting ω as the continuation parameter as before results in the bifurcation diagram in Fig. 18. It can be seen that the red branch is now stable at high frequencies, indicating a much more degraded controller. Furthermore, the oscillation amplitude of the tailplane is noticeably larger, which is another indication of the poor performance due to the lack of the high pass filter.

CONCLUSION

The use of harmonically-forced bifurcation analysis to analyse a classical extremum seeking controller has been presented. It has been shown that bifurcation diagrams provide a graphical representation of the system's dynamics. The nonlinear behaviours observed, including the coexistence of multiple solutions and loss of stability, highlight the link between extremum seeking control and dynamical system theory. Continuation can therefore be an intuitive tool for engineers to gain insight into the behaviour of extremum seeking control.

In the context of classical extremum seeking, continuation not only provides a method to systematically characterise the closed-loop dynamics, but can also be used to aid controller tuning by running a series of parameter sweeps. This provides significant savings in computation times comparing to relying purely on time simulations for verification. Although the same argument has been made in previous studies on equilibrium bifurcation analysis (no harmonic forcing) [48], it is even more important for extremum seeking applications, in which the dynamics of the plant and the forcing signal can span very different time scales.

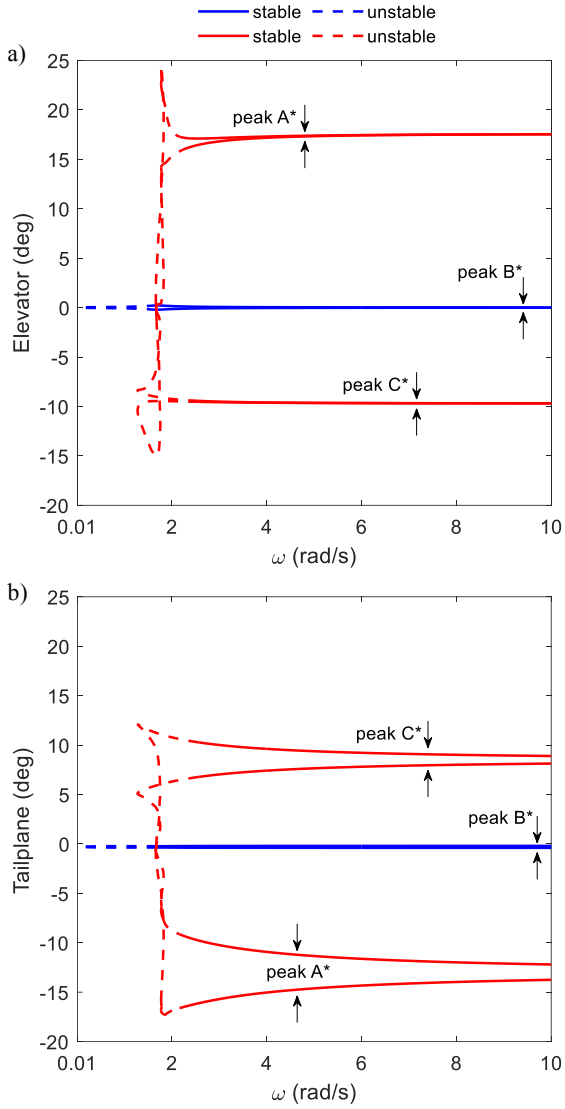

Fig. 18 Bifurcation diagram – no high-pass filter.

ACKNOWLEDGMENT

We are grateful to NASA Langley Research Center, specifically Kevin Cunningham and Gautam Shah, for providing the GTT model.

REFERENCES

[1] Y. Tan, W. H. Moase, C. Manzie, D. Nešić, and I. M. Y. Mareels, "Extremum seeking from 1922 to 2010," in *Proceedings of the 29th Chinese Control Conference*, 29-31 July 2010 2010, pp. 14-26.

[2] M. Krstić and H.-H. Wang, "Stability of extremum seeking feedback for general nonlinear dynamic systems," *Automatica,* vol. 36, no. 4, pp. 595-601, 2000/04/01/ 2000, doi: 10.1016/S0005-1098(99)00183-1.

[3] W. Hsin-Hsiung, S. Yeung, and M. Krstić, "Experimental application of extremum seeking on an axial-flow compressor,"

IEEE Transactions on Control Systems Technology, vol. 8, no. 2, pp. 300-309, 2000, doi: 10.1109/87.826801.

[4] J.-H. Chen, H.-T. Yau, and W. Hung, "Design and Study on Sliding Mode Extremum Seeking Control of the Chaos Embedded Particle Swarm Optimization for Maximum Power Point Tracking in Wind Power Systems," *Energies,* vol. 7, no. 3, pp. 1706-1720, 2014, doi: 10.3390/en7031706.

[5] P. Binetti, K. B. Ariyur, M. Krstić, and F. Bernelli, "Formation Flight Optimization Using Extremum Seeking Feedback," *Journal of Guidance, Control, and Dynamics,* vol. 26, no. 1, pp. 132-142, 2003, doi: 10.2514/2.5024.

[6] N. Killingsworth and M. Krstić, "Auto-tuning of PID controllers via extremum seeking," in *Proceedings of the 2005, American Control Conference, 2005.*, 8-10 June 2005 2005, pp. 2251-2256 vol. 4, doi: 10.1109/ACC.2005.1470304.

[7] W. Hsin-Hsiung and M. Krstić, "Extremum seeking for limit cycle minimization," *IEEE Transactions on Automatic Control,* vol. 45, no. 12, pp. 2432-2436, 2000, doi: 10.1109/9.895589.

[8] D. Nešić, "Extremum Seeking Control: Convergence Analysis," *European Journal of Control,* vol. 15, no. 3, pp. 331-347, 2009/01/01/ 2009, doi: 10.3166/ejc.15.331-347.

[9] M. Haring, N. van de Wouw, and D. Nešić, "Extremum-seeking control for nonlinear systems with periodic steady-state outputs," *Automatica,* vol. 49, no. 6, pp. 1883-1891, 2013/06/01/ 2013, doi: doi.org/10.1016/j.automatica.2013.02.061.

[10] MathWorks. "Simulink Control Design Release Notes." https://uk.mathworks.com/help/slcontrol/release-notes.html (accessed 21 February, 2022).

[11] L. Dewasme and A. Vande Wouwer, "Model-Free Extremum Seeking Control of Bioprocesses: A Review with a Worked Example," *Processes,* vol. 8, no. 10, 2020, doi: 10.3390/pr8101209.

[12] K. B. Ariyur and M. Krstić, *Real-Time Optimization by Extremum-Seeking Control*, 1 ed. (Real-Time Optimization by Extremum-Seeking Control). John Wiley & Sons, 2003.

[13] C. Zhang and R. Ordonez, *Extremum-Seeking Control and Applications A Numerical Optimization-Based Approach*, 1 ed. (Advances in Industrial Control). London: Springer, 2012, p. 201.

[14] H.-B. Dürr, M. S. Stanković, C. Ebenbauer, and K. H. Johansson, "Lie bracket approximation of extremum seeking systems," *Automatica,* vol. 49, no. 6, pp. 1538-1552, 2013/06/01/ 2013, doi: 10.1016/j.automatica.2013.02.016.

[15] V. Grushkovskaya, H.-B. Dürr, C. Ebenbauer, and A. Zuyev, "Extremum Seeking for Time-Varying Functions using Lie Bracket Approximations," in *IFAC-PapersOnLine*, 2017/07/01/ 2017, vol. 50, no. 1, pp. 5522-5528, doi: 10.1016/j.ifacol.2017.08.1093.

[16] M. Abdelgalil and H. Taha, "Lie bracket approximation-based extremum seeking with vanishing input oscillations," *Automatica,* vol. 133, p. 109735, 2021/11/01/ 2021, doi: 10.1016/j.automatica.2021.109735.

[17] O. Trollberg, B. Carlsson, and E. W. Jacobsen, "Extremum seeking control of the CANON process—Existence of multiple stationary solutions," *Journal of Process Control,* vol. 24, no. 2, pp. 348-356, 2014/02/01/ 2014, doi: 10.1016/j.jprocont.2013.11.007.

[18] O. Trollberg and E. W. Jacobsen, "On Bifurcations of the Zero Dynamics - Connecting Steady-State Optimality to Process Dynamics," in *IFAC-PapersOnLine*, 2015/01/01/ 2015, vol. 48, no. 8, pp. 170-175, doi: 10.1016/j.ifacol.2015.08.176.

[19] O. Trollberg and E. W. Jacobsen, "Non-Uniqueness of Stationary Solutions in Extremum Seeking Control," 2018.

[20] O. Trollberg, "On Real-Time Optimization using Extremum Seeking Control and Economic Model Predictive Control with Applications to Bioreactors and Paper Machines," Doctor of Philosophy, School of Electrical Engineering, KTH Royal Institute of Technology, Stockholm, 2017.

[21] E. J. Doedel. "AUTO-07P, Continuation and Bifurcation Software for Ordinary Differential Equations, Ver. 07P." California Institute of Technology and Concordia University. http://www.macs.hw.ac.uk/~gabriel/auto07/auto.html (accessed 21 February, 2022).

[22] h. fschild. "Continuation Core and Toolboxes (COCO) " https://sourceforge.net/p/cocotools/wiki/Home/ (accessed 13 July, 2022).

[23] M. A. Rotea, "Analysis of multivariable extremum seeking algorithms," in *Proceedings of the 2000 American Control Conference. ACC (IEEE Cat. No.00CH36334)*, 28-30 June 2000 2000, vol. 1: IEEE, 6 ed., pp. 433-437, doi: 10.1109/ACC.2000.878937.

[24] Z. Wu, C. W. Wong, and Y. Zhou, "Dual-Input/Single-Output Extremum-Seeking System for Jet Control," *AIAA Journal,* vol. 56, no. 4, pp. 1463-1471, 2018, doi: 10.2514/1.J056675.

[25] K. B. Ariyur and M. Krstic, "Slope seeking and application to compressor instability control," in *Proceedings of the 41st IEEE Conference on Decision and Control, 2002.*, Las Vegas, NV, 10-13 Dec. 2002 2002, vol. 4: IEEE, pp. 3690-3697, doi: 10.1109/CDC.2002.1184937.

[26] R. D. Brackston, A. Wynn, and J. F. Morrison, "Extremum seeking to control the amplitude and frequency of a pulsed jet for bluff body drag reduction," *Experiments in Fluids,* vol. 57, no. 10, p. 159, 2016/09/23 2016, doi: 10.1007/s00348-016-2243-4.

[27] T. R. Oliveira, M. Krstić, and D. Tsubakino, "Extremum Seeking for Static Maps With Delays," *IEEE Transactions on Automatic Control,* vol. 62, no. 4, pp. 1911-1926, 2017, doi: 10.1109/TAC.2016.2564958.

[28] D. Tsubakino, T. R. Oliveira, and M. Krstic, "Extremum Seeking Under Distributed Input Delay," *IFAC-PapersOnLine,* vol. 53, no. 2, pp. 5423-5428, 2020/01/01/ 2020, doi: 10.1016/j.ifacol.2020.12.1538.

[29] T. R. Oliveira, J. Feiling, S. Koga, and M. Krstić, "Multivariable Extremum Seeking for PDE Dynamic Systems," *IEEE Transactions on Automatic Control,* vol. 65, no. 11, pp. 4949-4956, 2020, doi: 10.1109/TAC.2020.3005177.

[30] T. R. Oliveira and M. Krstic, "Extremum seeking boundary control for PDE–PDE cascades," *Systems & Control Letters,* vol. 155, p. 105004, 2021/09/01/ 2021, doi: 10.1016/j.sysconle.2021.105004.

[31] J. I. Poveda and A. R. Teel, "A framework for a class of hybrid extremum seeking controllers with dynamic inclusions," *Automatica,* vol. 76, pp. 113-126, 2017/02/01/ 2017, doi: 10.1016/j.automatica.2016.10.029.

[32] J. I. Poveda, R. Kutadinata, C. Manzie, D. Nešić, A. R. Teel, and C. Liao, "Hybrid Extremum Seeking for Black-Box Optimization in Hybrid Plants: An Analytical Framework," in *2018 IEEE Conference on Decision and Control (CDC)*, 17-19 Dec. 2018 2018, pp. 2235-2240, doi: 10.1109/CDC.2018.8618907.

[33] H. Malek and Y. Chen, "Fractional Order Extremum Seeking Control: Performance and Stability Analysis," *IEEE/ASME Transactions on Mechatronics,* vol. 21, no. 3, pp. 1620-1628, 2016, doi: 10.1109/TMECH.2016.2517621.

[34] H. Malek, S. Dadras, and Y. Chen, "Performance analysis of fractional order extremum seeking control," *ISA Transactions,* vol. 63, pp. 281-287, 2016/07/01/ 2016, doi: 10.1016/j.isatra.2016.02.024.

[35] K. Cunningham *et al.*, "Preliminary Test Results for Stability and Control Characteristics of a Generic T-tail Transport Airplane at High Angle of Attack," presented at the 2018 AIAA Atmospheric Flight Mechanics Conference, Kissimmee, Florida, 8-12 January 2018, 2018, AIAA-2018-0529.

[36] K. Cunningham, G. H. Shah, M. A. Hill, B. P. Pickering, J. S. Litt, and S. Norin, "A Generic T-tail Transport Airplane Simulation for High-Angle-of-Attack Dynamics Modeling Investigations," presented at the 2018 AIAA Modeling and Simulation Technologies Conference, Kissimmee, Florida, 8-12 January 2018, 2018, AIAA-2018-1168.

[37] K. Cunningham, G. H. Shah, P. C. Murphy, M. A. Hill, and B. Pickering, "Pilot Sensitivity to Simulator Flight Dynamics Model Formulation for Stall Training," presented at the AIAA Scitech 2019 Forum, San Diego, California, 7-11 January 2019, 2019, AIAA-2019-0717.

[38] Y. Didenko *et al.*, "The specific features of FBW control laws of advanced regional jet," in *IFAC Proceedings Volumes*, 2007/01/01/ 2007, vol. 40, no. 7, pp. 129-134, doi: 10.3182/20070625-5-FR-2916.00023.

[39] F. Holzapfel, M. Heller, M. Weingartner, G. Sachs, and O. da Costa, "Development of control laws for the simulation of a new transport aircraft," *Proceedings of the Institution of Mechanical Engineers, Part G: Journal of Aerospace Engineering,* vol. 223, no. 2, pp. 141-156, 2009, doi: 10.1243/09544100jaero309.

[40] D. Niedermeier and A. A. Lambregts, "Fly-by-wire augmented manual control - Basic design considerations," in *28th International Congress of the Aeronautical Sciences*, Brisbane, Australia, 23-28 September 2012: ICAS.

[41] B. Krauskopf, H. M. Osinga, and J. Galán-Vioque, "Numerical continuation methods for dynamical systems: path following and boundary value problems," in *Understanding Complex Systems*, J. A. S. Kelso Ed., (Springer complexity. Dordrecht: Springer, 2007, ch. 1.

[42] D. H. Nguyen, M. G. Goman, M. H. Lowenberg, and S. A. Neild, "Evaluating Longitudinal Unsteady Aerodynamic Effects in Stall for a T-Tail Transport Model," *Journal of Aircraft,* vol. 59, no. 4, pp. 964-976, July 2022, doi: 10.2514/1.C036622.

[43] D. H. Nguyen, M. H. Lowenberg, and S. A. Neild, "Frequency-Domain Bifurcation Analysis of a Nonlinear Flight Dynamics Model," *Journal of Guidance, Control, and Dynamics,* vol. 44, no. 1, pp. 138-150, January 2021, doi: 10.2514/1.G005197.

[44] E. Coetzee, B. Krauskopf, and M. H. Lowenberg, "The Dynamical Systems Toolbox: Integrating AUTO into Matlab," presented at the 16th US National Congress of Theoretical and Applied Mechanics, State College, PA, 27 June-2 July 2010, 2010, USNCTAM2010-827.

[45] E. Doedel, H. B. Keller, and J. P. Kernevez, "Numerical analysis and control of bifurcation problems (I): Bifurcation in finite dimensions," *International Journal of Bifurcation and Chaos,* vol. 01, no. 03, pp. 493-520, 1991, doi: 10.1142/s0218127491000397.

[46] E. Doedel, H. B. Keller, and J. P. Kernevez, "Numerical analysis and control of bifurcation problems (II): Bifurcation in infinite dimensions," *International Journal of Bifurcation and Chaos,* vol. 01, no. 04, pp. 745-772, 1991, doi: 10.1142/s0218127491000555.

[47] D. H. Nguyen, M. H. Lowenberg, and S. A. Neild, "Analysing Dynamic Deep Stall Recovery Using a Nonlinear Frequency Approach," *Nonlinear Dynamics,* vol. 108, no. 2, pp. 1179–1196, April 2022, doi: 10.1007/s11071-022-07283-z.

[48] S. Sharma, E. B. Coetzee, M. H. Lowenberg, S. A. Neild, and B. Krauskopf, "Numerical continuation and bifurcation analysis in aircraft design: an industrial perspective," *Philosophical Transactions of the Royal Society A: Mathematical, Physical and Engineering Sciences,* vol. 373, no. 2051, p. 20140406, 2015, doi: 10.1098/rsta.2014.0406.

Duc H. Nguyen received an M.Eng. degree in 2019 and a Ph.D. degree in 2021 in aerospace engineering from the University of Bristol, Bristol, U.K.

Since then, he has held both post-doctoral teaching and research roles at the Department of Aerospace Engineering – University of Bristol. Dr. Nguyen's research experience includes flight dynamics and control, nonlinear dynamics, bifurcation methods, and automatic control of composites manufacturing. He is also a lead tutor for the University of Cambridge's online course in control engineering.

Mark H. Lowenberg Mark H Lowenberg has BSc and MSc Aeronautical Engineering degrees from the University of the Witwatersrand in Johannesburg and a PhD from the University of Bristol in the UK. After working at the Council for Scientific & Industrial Research (CSIR) and then the University of the Witwatersrand in South Africa, he joined the University of Bristol in 1992. He has held the post of Professor of Flight Dynamics since 2014. His research interests include nonlinear problems in aerospace, especially flight dynamics and control, numerical continuation and bifurcation analysis, and novel dynamic wind tunnel test techniques.

Simon A. Neild Simon A. Neild received a MEng in Engineering Science and a DPhil in Engineering at the University of Oxford (in 1998 and 2001 respectively). He then joined the University of Bristol and since 2013 has held the position of Professor in Nonlinear Structural Dynamics. His research spans vibration control, developing novel experimental methods and nonlinear analysis of structures including the use of continuation, perturbation techniques and reduced-order modelling. He is currently the Head of School for Civil, Aerospace and Mechanical Engineering (CAME) at the University.